

Supporting Information

**Fluorescence “ON-OFF-ON” Response in the Formation of a Tetrahedral
Anionocage and Encapsulation of Halogenated Hydrocarbons**

Jie Zhao,^{a, b#} Wenyao Zhang,^{b#} Yayun Zheng,^{b#} Yue Wang,^b Dong Yang^{b*}

^a School of Chemistry and Chemical Engineering, Xi'an University of Architecture and Technology, Xi'an 710055, China

^b Key Laboratory of Synthetic and Natural Functional Molecule of the Ministry of Education, College of Chemistry and Materials Science, Northwest University, Xi'an 710069, China

E-mail: yangdong@nwu.edu.cn

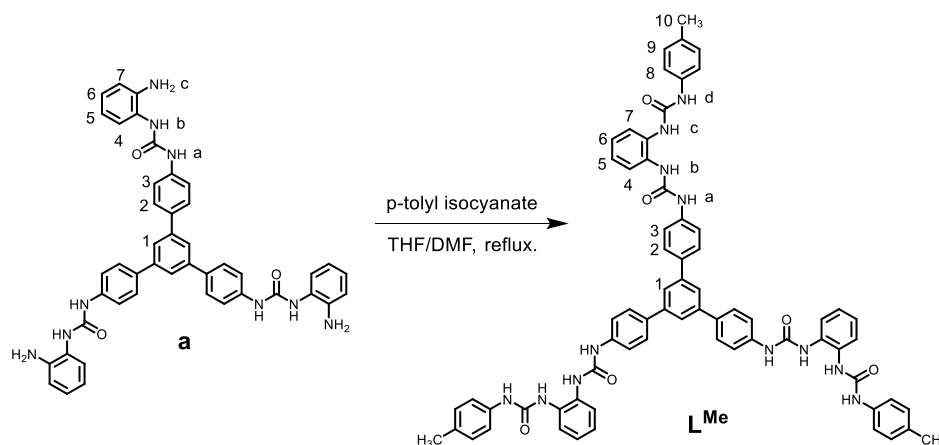
Table of Contents:

- S1. General considerations**
 - S2. Synthesis of L^{NO2}, L^{Me} and cage 1^{Me}**
 - S3. ¹H NMR spectroscopy**
 - S4. Fluorescence property**
 - S5. UV-vis property**
 - S6. X-ray crystallography**
 - S7. High-Resolution MS Study**
 - S8. Reference**
-

S1. General considerations

The *p*-tolyl isocyanate was purchased from Alfa Aesar and used as received. All solvents and other reagents were of reagent grade quality and purchased commercially. ^1H and ^{13}C NMR spectra were recorded on a Varian unity INOVA-400 spectrometer at 400, and 100 MHz, respectively, using TMS as an internal standard for ^1H and ^{13}C .

S2. Synthesis of ligand L^{NO_2} , L^{Me} and cage 1^{Me}



L^{NO_2}

L^{NO_2} was synthesized according to the literature procedures.¹

L^{Me}

Compound \mathbf{a}^1 (0.3 g, 0.4 mmol) was dissolved in 6 mL of DMF and the solution was added dropwise into a 10 mL THF solution of *p*-tolyl isocyanate (0.45 g, 2.7 mmol). The mixture was refluxed for 24 hours and the precipitate thus obtained was filtered off and washed with toluene and diethyl ether and then dried over vacuum to yield a yellow solid (0.39 g, 0.34 mmol, 84 %). ^1H NMR (400 MHz, $\text{DMSO-}d_6$): δ 9.24 (s, 1H, NHa), 8.97 (s, 1H, NHb), 8.10 (s, 1H, NHc), 8.04 (s, 1H, NHd), 7.79 (d, $J = 8.0$ Hz, 3H, H1/H3), 7.62 (m, 4H, H2/H4/H7), 7.35 (s, $J = 8.0$ Hz, 2H, H8), 7.09 (m, 4H, H5/H6/H9), 2.23 (s, 3H, H10); ^{13}C NMR (100 MHz, $\text{DMSO-}d_6$): 153.3 (CO), 153.2 (CO), 141.2 (C), 139.6 (C), 137.3 (C), 133.6 (C), 131.4 (C), 131.2 (C), 130.6 (C), 129.2 (CH), 127.5 (CH), 124.1 (CH), 124.0 (CH), 123.9 (CH), 122.6 (CH), 118.5 (CH), 118.3 (CH), 20.4 (CH_3). IR (KBr, v/cm^{-1}): 3306 (NH), 1635 (CO), 1607 (CO), 1556, 1512, 1450, 1402, 1314, 1291, 1241, 1104, 892, 812, 742, 675, 569, 501, 465. ESI-MS: m/z 1153.45, calculated for $\text{C}_{69}\text{H}_{61}\text{N}_{12}\text{O}_6$ [$\text{M} + \text{H}$] 1153.48; 1175.44, calculated for $\text{C}_{69}\text{H}_{60}\text{N}_{12}\text{O}_6\text{Na}$ [$\text{M} + \text{Na}$] 1175.46.

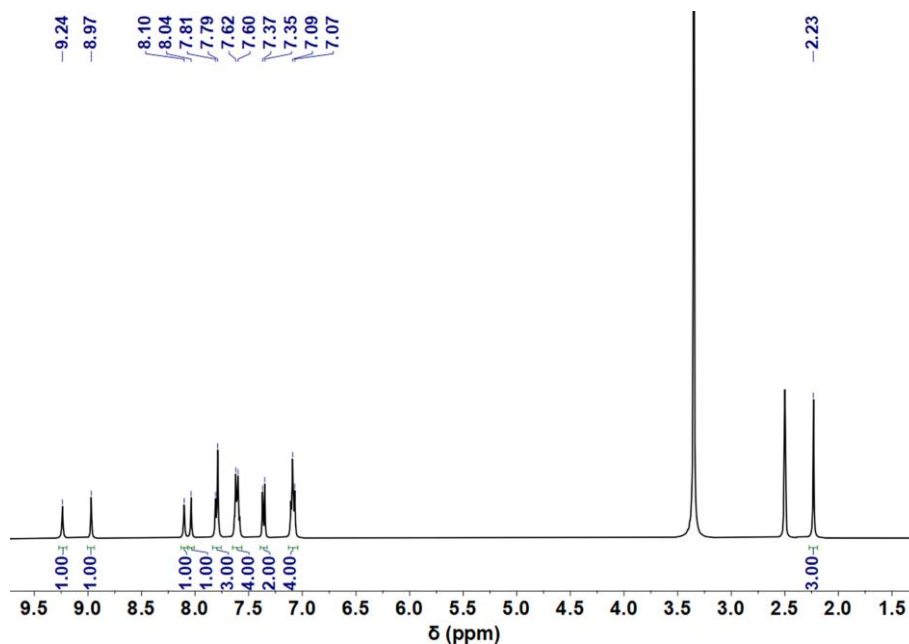


Figure S1. ^1H NMR spectrum (400 MHz, $\text{DMSO-}d_6$, 298 K) of L^{Me} .

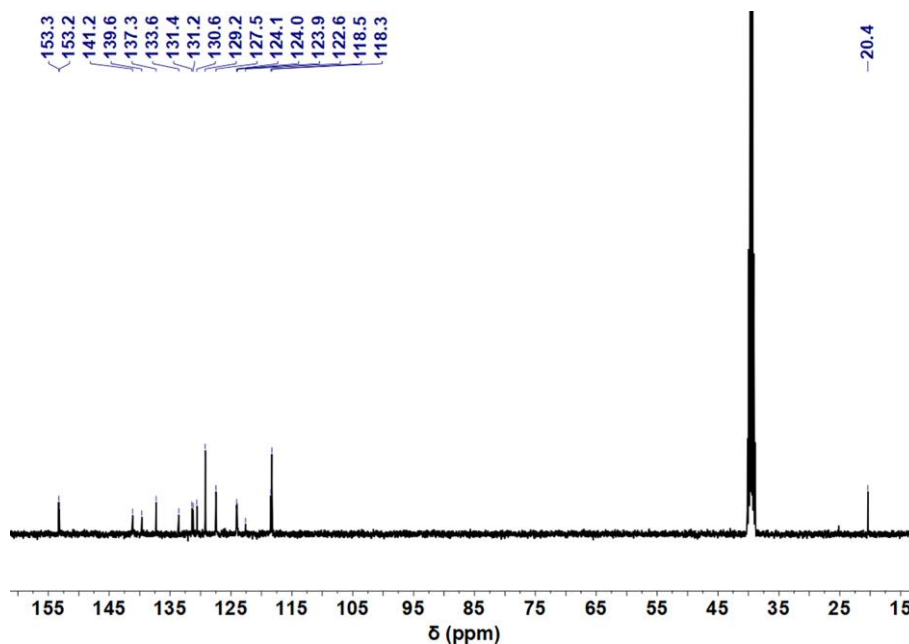


Figure S2. ^{13}C NMR spectrum (100 MHz, $\text{DMSO-}d_6$, 298 K) of L^{Me} .

Cage $\mathbf{1}^{\text{Me}}$

The synthesis of cage $\mathbf{1}^{\text{Me}}$: $(\text{TBA})_3\text{PO}_4$ (13 μL , 0.625 mol/L; generated in situ from $(\text{TBA})\text{OH}$ and H_3PO_4 in water) was added to a suspension of L^{Me} (10 mg, 8 μmol) in acetone (1 mL). After stirring overnight at room temperature, centrifuged to collect clear colorless solution. Slow vapor diffusion of diethyl ether into this solution provided colorless crystals of cage $\mathbf{1}^{\text{Me}}$ within two weeks.

S3. ^1H NMR spectroscopy

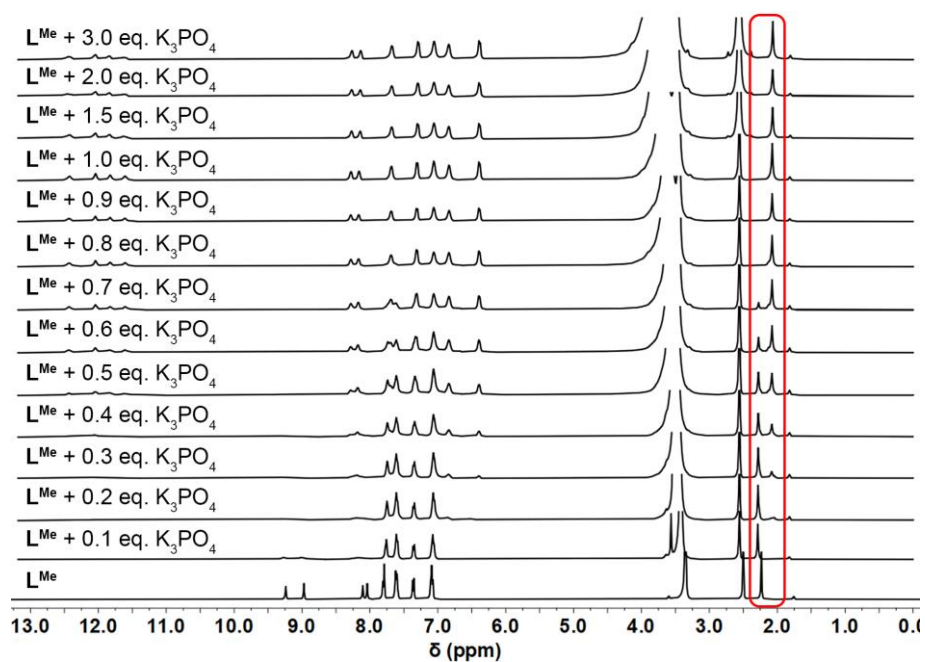


Figure S3. ^1H NMR titration (400 MHz, $\text{DMSO-}d_6$, 298 K) of L^{Me} (5 mM) with $[\text{K}(\text{[18]crown-6})_3\text{PO}_4]$.

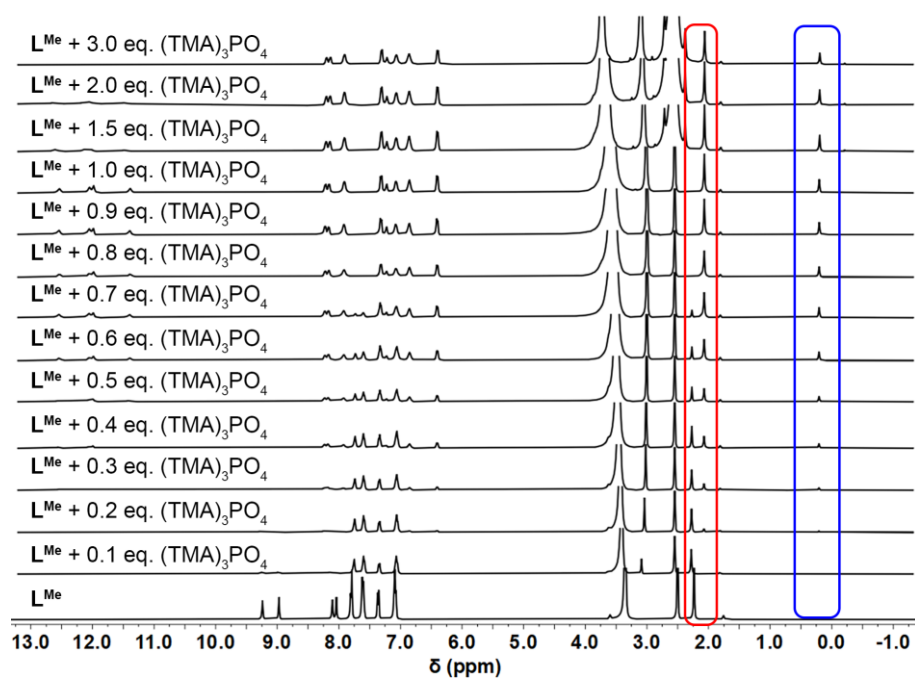


Figure S4. ^1H NMR titration (400 MHz, $\text{DMSO-}d_6$, 298 K) of L^{Me} (5 mM) with $(\text{TMA})_3\text{PO}_4$.

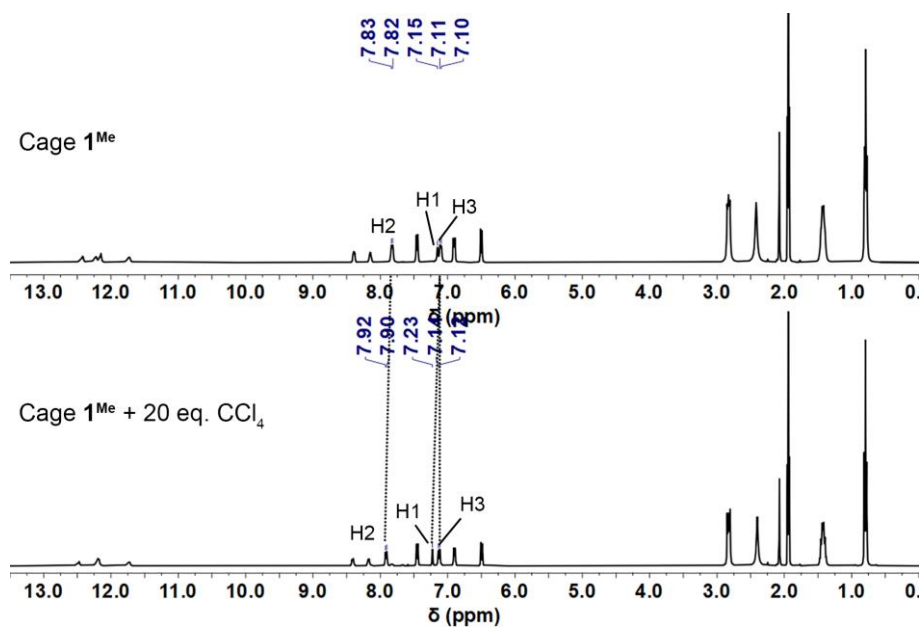


Figure S5. ^1H NMR spectra (400 MHz, CD_3CN , 298 K) of $(\text{TPA})_{12}[(\text{PO}_4)_4(\text{L}^{\text{Me}})_4]\text{CH}_3\text{CN}$ ($\mathbf{1}^{\text{Me}}\text{CH}_3\text{CN}$) (top, 1 mM) and $(\text{TPA})_{12}[(\text{PO}_4)_4(\text{L}^{\text{Me}})_4]\text{CH}_3\text{CN}$ ($\mathbf{1}^{\text{Me}}\text{CH}_3\text{CN}$) with 20 eq. CCl_4 (bottom).

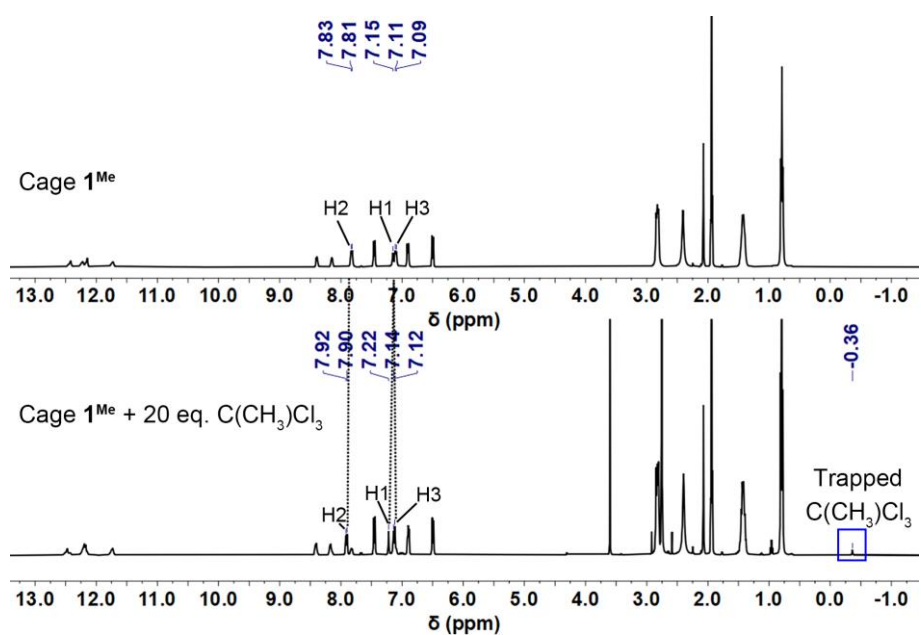


Figure S6. ^1H NMR spectra (400 MHz, CD_3CN , 298 K) of $(\text{TPA})_{12}[(\text{PO}_4)_4(\text{L}^{\text{Me}})_4]\text{CH}_3\text{CN}$ ($\mathbf{1}^{\text{Me}}\text{CH}_3\text{CN}$) (top, 1 mM) and $(\text{TPA})_{12}[(\text{PO}_4)_4(\text{L}^{\text{Me}})_4]\text{CH}_3\text{CN}$ ($\mathbf{1}^{\text{Me}}\text{CH}_3\text{CN}$) with 20 eq. $\text{C}(\text{CH}_3)\text{Cl}_3$ (bottom).

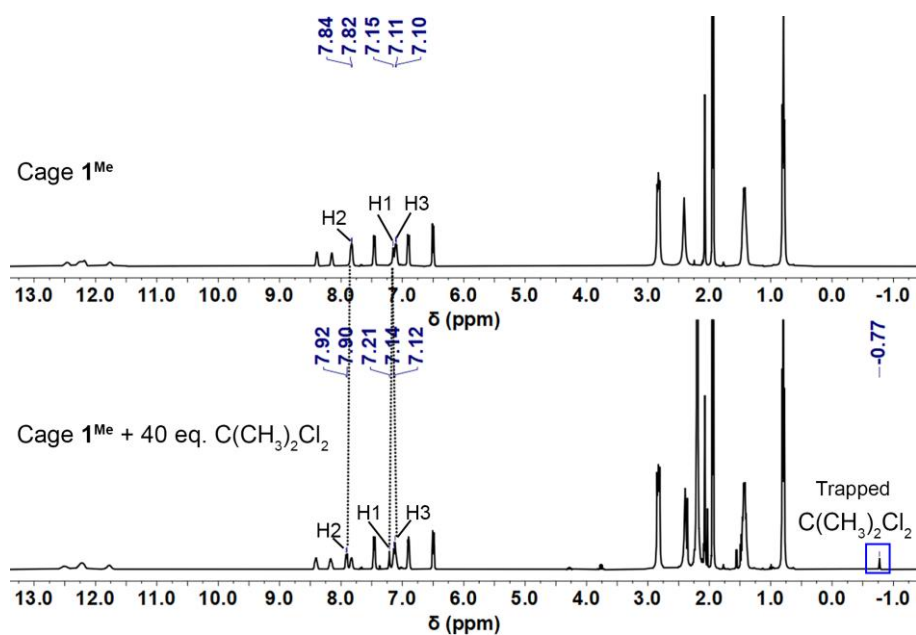


Figure S7. ^1H NMR spectra (400 MHz, CD_3CN , 298 K) of $(\text{TPA})_{12}[(\text{PO}_4)_4(\text{L}^{\text{Me}})_4]\text{CH}_3\text{CN}$ ($\mathbf{1}^{\text{Me}}\text{CH}_3\text{CN}$) (top, 1 mM) and $(\text{TPA})_{12}[(\text{PO}_4)_4(\text{L}^{\text{Me}})_4]\text{CH}_3\text{CN}$ ($\mathbf{1}^{\text{Me}}\text{CH}_3\text{CN}$) with 40 eq. $\text{C}(\text{CH}_3)_2\text{Cl}_2$ (bottom).

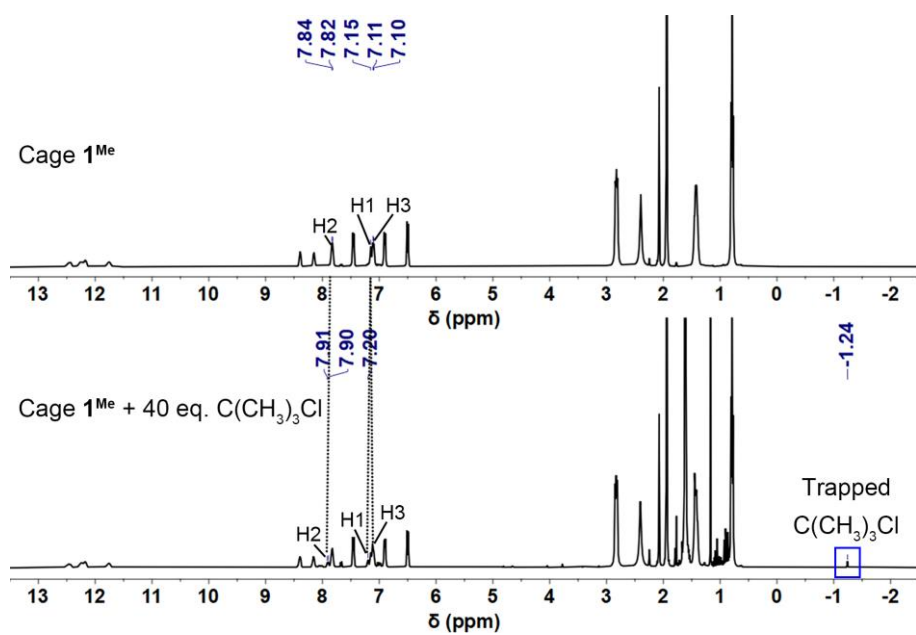


Figure S8. ^1H NMR spectra (400 MHz, CD_3CN , 298 K) of $(\text{TPA})_{12}[(\text{PO}_4)_4(\text{L}^{\text{Me}})_4]\text{CH}_3\text{CN}$ ($\mathbf{1}^{\text{Me}}\text{CH}_3\text{CN}$) (top, 1 mM) and $(\text{TPA})_{12}[(\text{PO}_4)_4(\text{L}^{\text{Me}})_4]\text{CH}_3\text{CN}$ ($\mathbf{1}^{\text{Me}}\text{CH}_3\text{CN}$) with 40 eq. $\text{C}(\text{CH}_3)_3\text{Cl}$ (bottom).

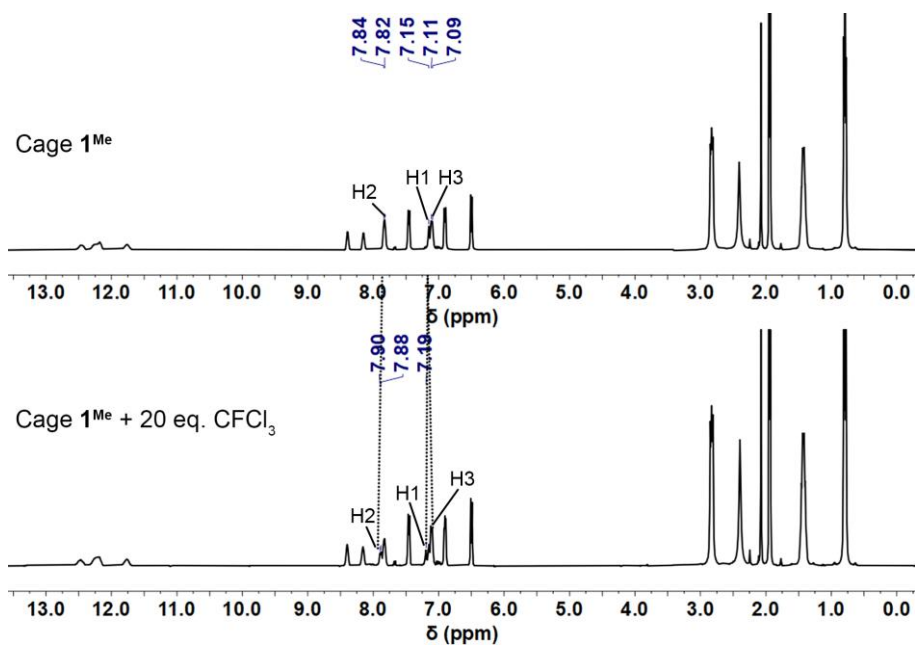


Figure S9. ^1H NMR spectra (400 MHz, CD_3CN , 298 K) of $(\text{TPA})_{12}[(\text{PO}_4)_4(\text{L}^{\text{Me}})_4\supset\text{CH}_3\text{CN}]$ ($\mathbf{1}^{\text{Me}}\supset\text{CH}_3\text{CN}$) (top, 1 mM) and $(\text{TPA})_{12}[(\text{PO}_4)_4(\text{L}^{\text{Me}})_4\supset\text{CH}_3\text{CN}]$ ($\mathbf{1}^{\text{Me}}\supset\text{CH}_3\text{CN}$) with 20 eq. CFCI_3 (bottom).

S4. Fluorescence property

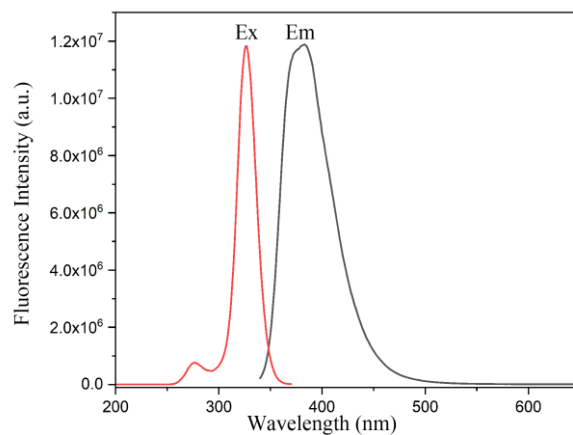


Figure S10. Fluorescence excitation and emission spectrum of L^{Me} (40 μM in DMSO).

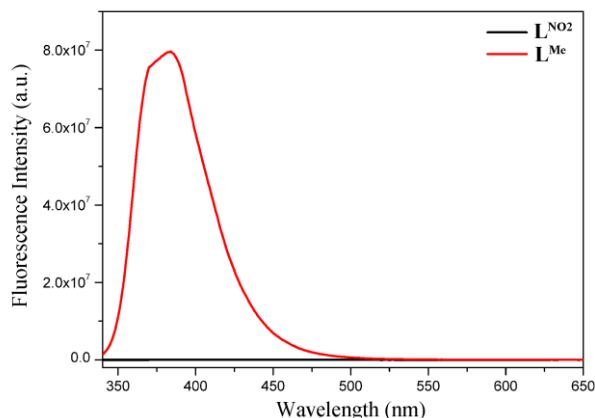


Figure S11. Fluorescence emission spectra of L^{NO_2} and L^{Me} ($40 \mu M$ in DMSO).

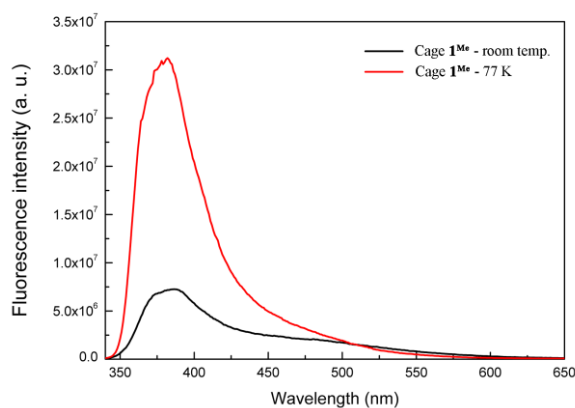


Figure S12. Fluorescence emission spectra of $(TPA)_{12}[(PO_4)_4(L^{Me})_4]CH_3CN$ ($1^{Me} = CH_3CN$) under room temperature and at 77 K ($40 \mu M$ in DMSO).

Binding constants studies

The binding constants were evaluated by fluorescence titrations. All the measurements were performed at room temperature. In the titrations, successive addition of known amounts of PO_4^{3-} anions or guests to a 3 mL solution of L^{Me} ($40 \mu M$, DMSO) or cage 1^{Me} ($10 \mu M$, CH_3CN).

The binding constant (Ka) and coefficient value (n) were calculated using the Hill equation.²

$$\theta = \frac{\Delta I}{\Delta I_{max}} \quad (S1)$$

$$\log \frac{\theta}{1-\theta} = n \log[G] + n \log Ka \quad (S2)$$

Where θ is the fraction of binding sites occupied by the guests (or PO_4^{3-}), $[G]$ is the

concentration of guest (or PO_4^{3-}), n is the Hill coefficient describing cooperativity, and K_a is the apparent association constant.

In the Hill equation, the value of θ was obtained using Equation S1. The value of θ was obtained by using the change of fluorescence intensity (ΔI) as compared against the maximum change of fluorescence intensity (ΔI_{max}).

Table S1. Binding constants (K_a , M^{-1}) of cage **1^{Me}** to different guests.

Guest	K_a/M^{-1}
$\text{C}(\text{CH}_3)_3\text{Cl}$	198 ± 1
$\text{C}(\text{CH}_3)_2\text{Cl}_2$	409 ± 1
$\text{C}(\text{CH}_3)\text{Cl}_3$	280 ± 2
CCl_4	693 ± 1
CFCl_3	391 ± 2
TMA^+	$(2.91 \pm 0.01) \times 10^5$

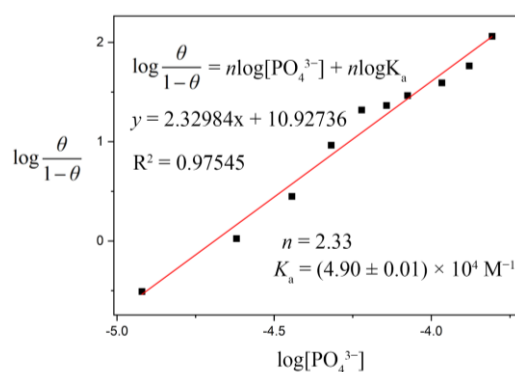


Figure S13. The $\log \frac{\theta}{1-\theta}$ vs $\log[\text{PO}_4^{3-}]$ in fluorescence titration of **L^{Me}** and PO_4^{3-} .

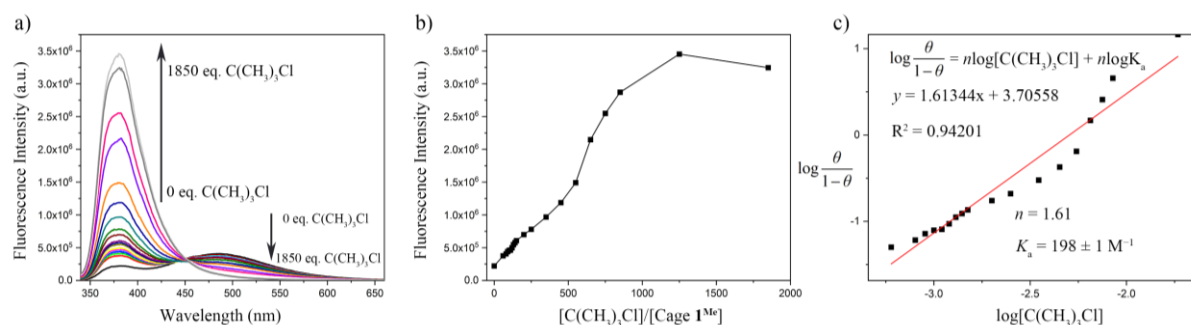


Figure S14. a) Fluorescence emission spectra ($\lambda_{\text{ex}}=335$) of cage **1^{Me}** (10 μM) in acetonitrile upon addition of $\text{C}(\text{CH}_3)_3\text{Cl}$, b) Fluorescence intensity vs $[\text{C}(\text{CH}_3)_3\text{Cl}]/[\text{Cage } \mathbf{1}^{\text{Me}}]$ and c) $\log \frac{\theta}{1-\theta}$ vs $\log[\text{C}(\text{CH}_3)_3\text{Cl}]$.

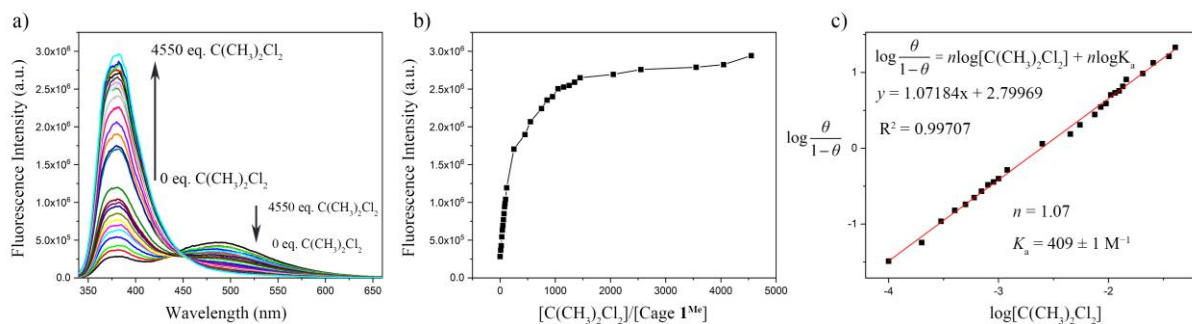


Figure S15. a) Fluorescence emission spectra ($\lambda_{\text{ex}}=335$) of cage **1^{Me}** (10 μM) in acetonitrile upon addition of $\text{C}(\text{CH}_3)_2\text{Cl}_2$, b) Fluorescence intensity vs $[\text{C}(\text{CH}_3)_2\text{Cl}_2]/[\text{Cage } \mathbf{1}^{\text{Me}}]$ and c) $\log \frac{\theta}{1-\theta}$ vs $\log[\text{C}(\text{CH}_3)_2\text{Cl}_2]$.

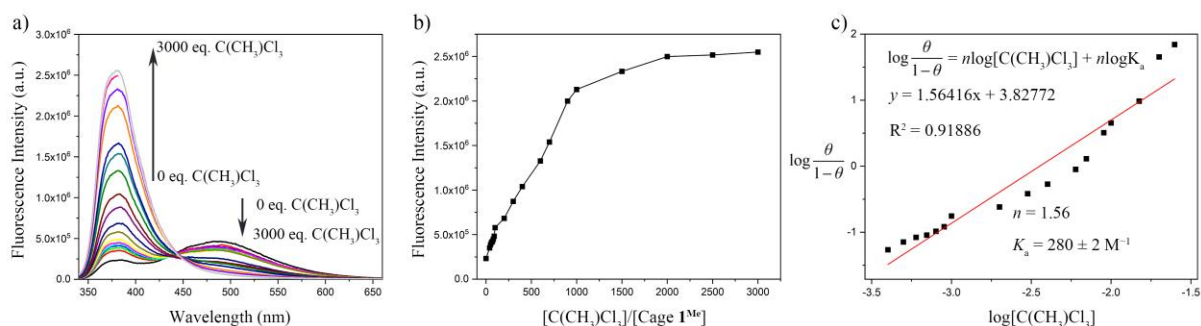


Figure S16. a) Fluorescence emission spectra ($\lambda_{\text{ex}}=335$) of cage **1^{Me}** (10 μM) in acetonitrile upon addition of $\text{C}(\text{CH}_3)\text{Cl}_3$, b) Fluorescence intensity vs $[\text{C}(\text{CH}_3)\text{Cl}_3]/[\text{Cage } \mathbf{1}^{\text{Me}}]$ and c) $\log \frac{\theta}{1-\theta}$ vs $\log[\text{C}(\text{CH}_3)\text{Cl}_3]$.

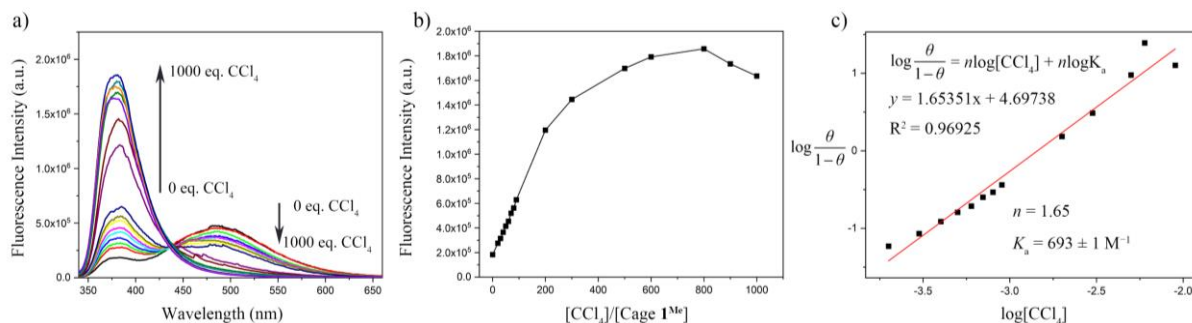


Figure S17. a) Fluorescence emission spectra ($\lambda_{\text{ex}}=335$) of cage **1^{Me}** (10 μM) in acetonitrile upon addition of CCl_4 , b) Fluorescence intensity vs $[\text{CCl}_4]/[\text{Cage } \mathbf{1}^{\text{Me}}]$ and c) $\log \frac{\theta}{1-\theta}$ vs $\log [\text{CCl}_4]$.

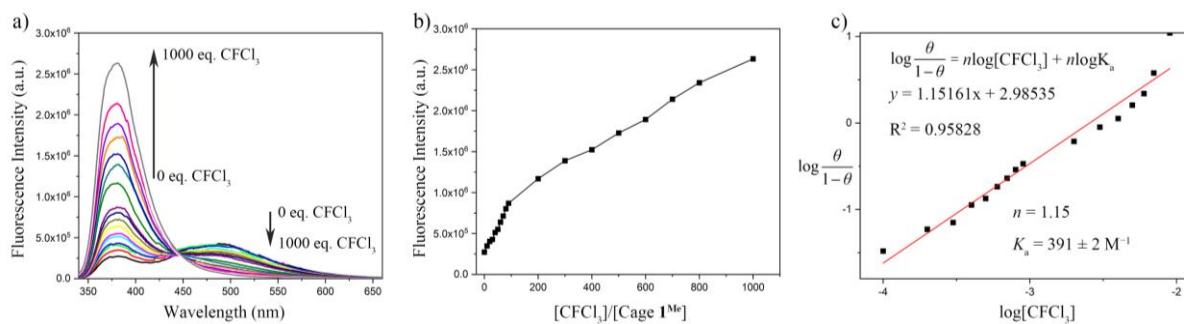


Figure S18. a) Fluorescence emission spectra ($\lambda_{ex}=335$) of cage 1^{Me} (10 μM) in acetonitrile upon addition of $CFC1_3$, b) Fluorescence intensity vs $[CFC1_3]/[Cage\ 1^{Me}]$ and c) $\log \frac{\theta}{1-\theta}$ vs $\log [CFC1_3]$.

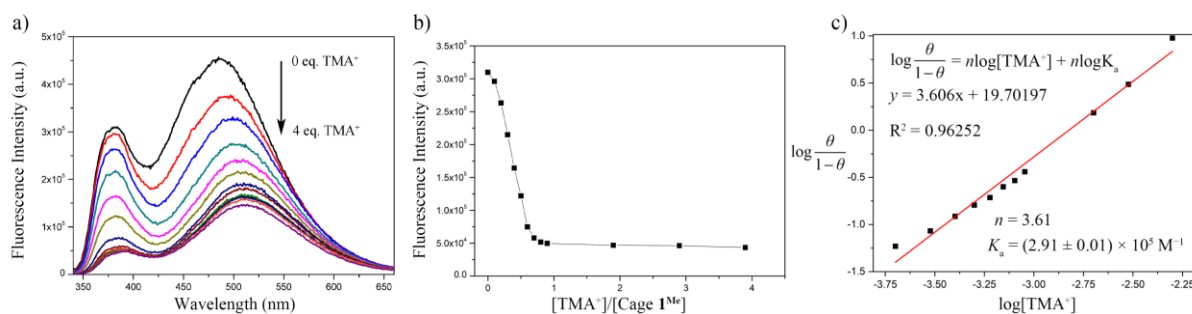


Figure S19. a) Fluorescence emission spectra ($\lambda_{ex}=335$) of cage 1^{Me} (10 μM) in acetonitrile upon addition of TMA^+ , b) Fluorescence intensity vs $[TMA^+]/[Cage\ 1^{Me}]$ and c) $\log \frac{\theta}{1-\theta}$ vs $\log [TMA^+]$.

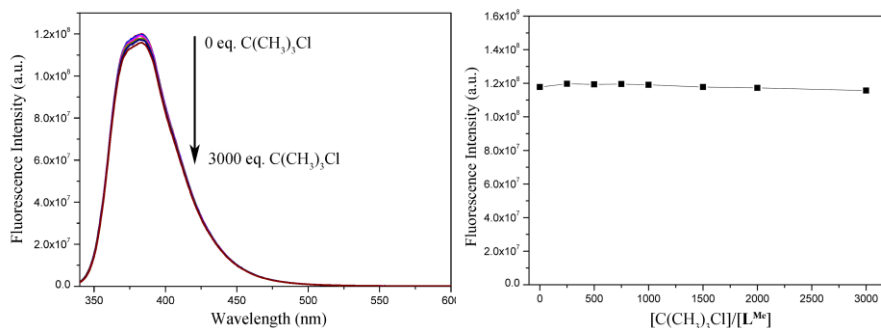


Figure S20. Fluorescence emission spectra ($\lambda_{ex}=335$) of L^{Me} (40 μM) in DMSO upon addition of $C(CH_3)_3Cl$.

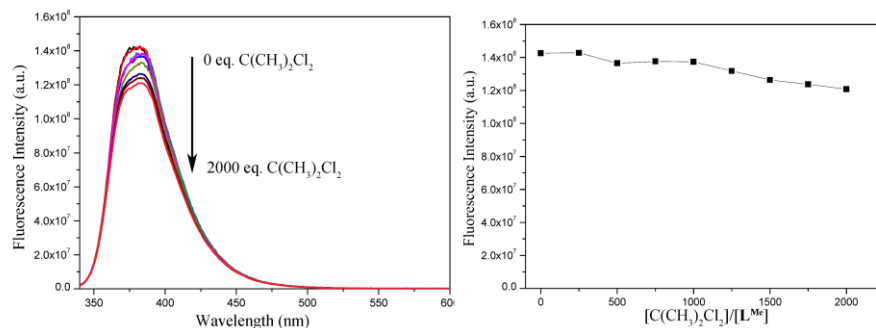


Figure S21. Fluorescence emission spectra ($\lambda_{ex}=335$) of L^{Me} (40 μM) in DMSO upon addition of $C(CH_3)_2Cl_2$.

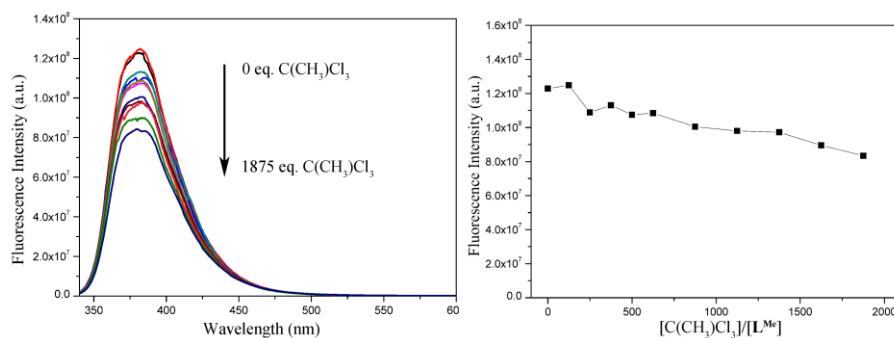


Figure S22. Fluorescence emission spectra ($\lambda_{\text{ex}}=335$) of L^{Me} ($40 \mu\text{M}$) in DMSO upon addition of $\text{C}(\text{CH}_3)\text{Cl}_3$.

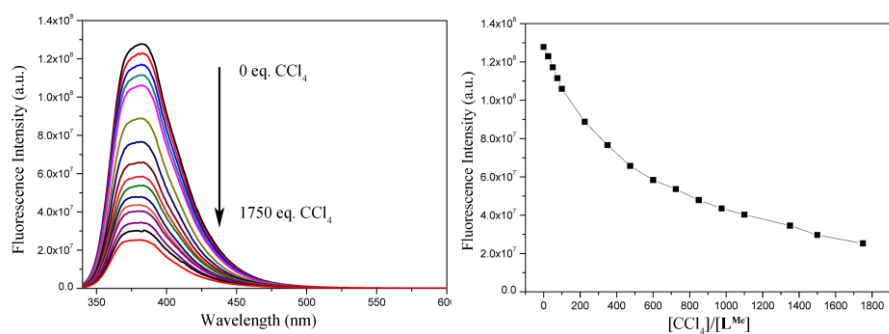


Figure S23. Fluorescence emission spectra ($\lambda_{\text{ex}}=335$) of L^{Me} ($40 \mu\text{M}$) in DMSO upon addition of CCl_4 .

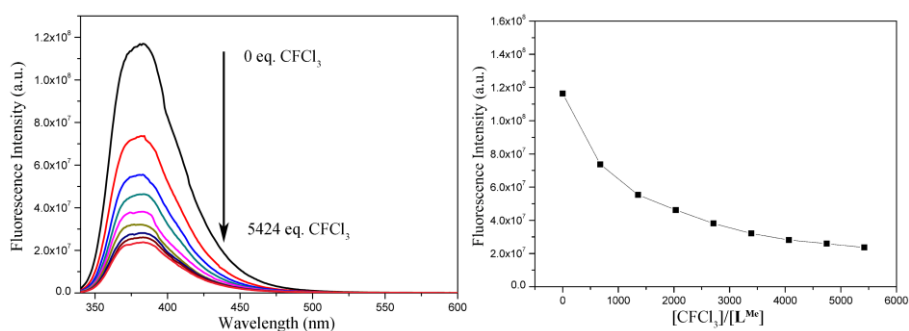


Figure S24. Fluorescence emission spectra ($\lambda_{\text{ex}}=335$) of L^{Me} ($40 \mu\text{M}$) in DMSO upon addition of CFCl_3 .

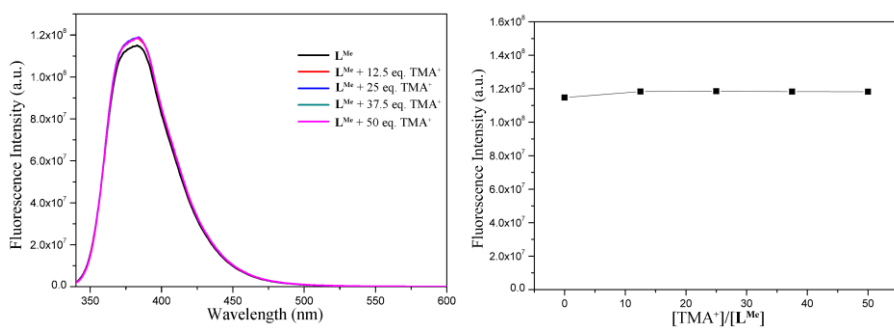


Figure S25. Fluorescence emission spectra ($\lambda_{\text{ex}}=335$) of L^{Me} ($40 \mu\text{M}$) in DMSO upon addition of TMA^+ .

Detection limits

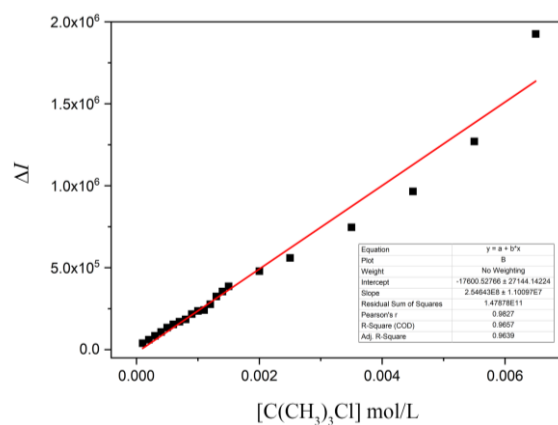


Figure S26. A plot of the difference of the fluorescence intensity (ΔI) at 381 nm versus the concentration of $C(CH_3)_3Cl$. Linear Equation: $y = (2.5 \times 10^8) x - 17600.5$, $R^2 = 0.9639$; $y = 0$, $x = 69.1 \mu M$.

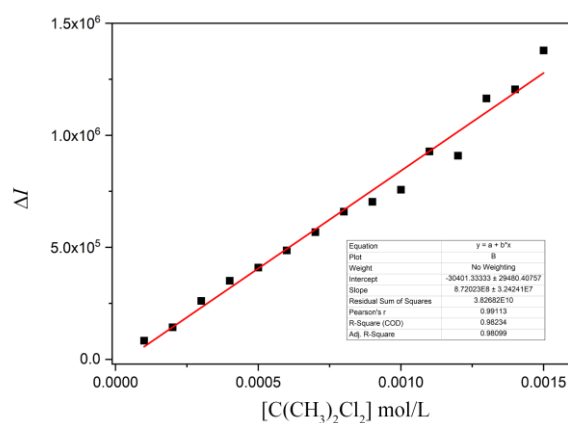


Figure S27. A plot of the difference of the fluorescence intensity (ΔI) at 381 nm versus the concentration of $C(CH_3)_2Cl_2$. Linear Equation: $y = (8.7 \times 10^8) x - 30401.3$, $R^2 = 0.98099$; $y = 0$, $x = 34.9 \mu M$.

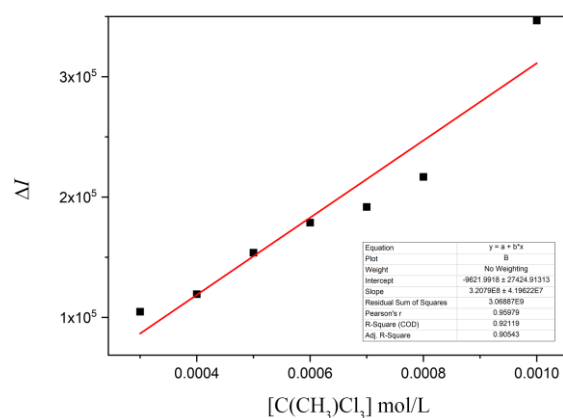


Figure S28. A plot of the difference of the fluorescence intensity (ΔI) at 381 nm versus the concentration of $C(CH_3)Cl_3$. Linear Equation: $y = (3.2 \times 10^8) x - 9622.0$, $R^2 = 0.90543$; $y = 0$, $x = 30.0 \mu M$.

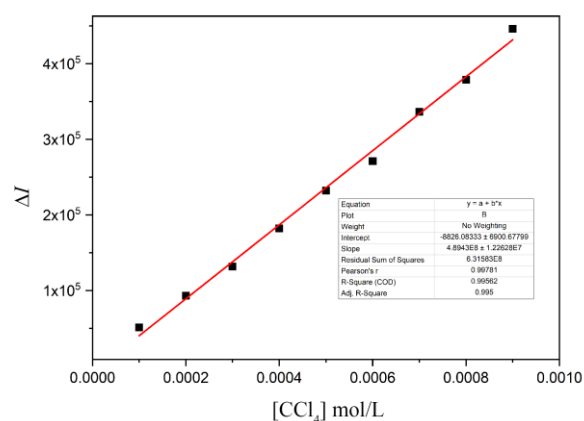


Figure S29. A plot of the difference of the fluorescence intensity (ΔI) at 381 nm versus the concentration of CCl_4 . Linear Equation: $y = (4.9 \times 10^8) x - 8826.1$, $R^2 = 0.995$; $y = 0$, $x = 18.0 \mu\text{M}$.

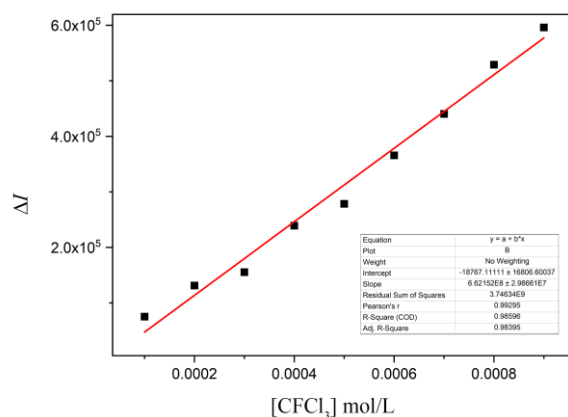


Figure S30. A plot of the difference of the fluorescence intensity (ΔI) at 381 nm versus the concentration of CFCl_3 . Linear Equation: $y = (6.6 \times 10^8) x - 18767.1$, $R^2 = 0.98395$; $y = 0$, $x = 28.3 \mu\text{M}$.

Binding of different anions

The binding ability of L^{Me} with various anions was examined by fluorescence spectra (tetra-*n*-butylammonium (TBA^+) as counter cation without special instructions). The addition of PO_4^{3-} anions caused significant fluorescence quenching. The other anions, such as NO_3^- , Br^- , Cl^- , I^- , and HSO_4^- induced no obvious change and SO_4^{2-} , CO_3^{2-} ($[\text{K}([\text{18}]\text{crown-6})]^+$ as counter cation), HCO_3^- ($[\text{Na}([\text{15}]\text{crown-5})]^+$ as counter cation), AcO^- , H_2PO_4^- and HPO_4^{2-} quenched fluorescence to some extent (Figure S31).

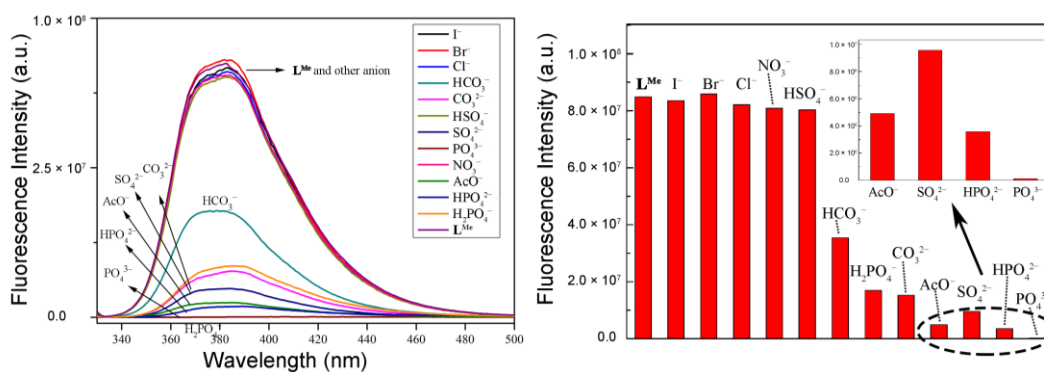


Figure S31. a) Fluorescence emission spectra ($\lambda_{exc} = 330$ nm) of L^{Me} (40 μ M in DMSO) upon addition of various anions (10 equiv); b) Variation of fluorescence intensity at $\lambda_{em} = 381$ nm.

Fluorescence lifetime

Fluorescence decay for L^{Me} at 380 nm, $A_4L_4(TBA)_{12}[(PO_4)_4(L^{Me})_4]$ (cage 1^{Me}) at 381 nm were measured (Figures S32, S33). Fluorescence decay measurements of L^{Me} at 380 nm showed a double-exponential behavior with lifetime of 0.42 ns and 4.75 ns. When L^{Me} coordinate with PO_4^{3-} anions to form cage 1^{Me} , the short-lived component (τ_1) is almost the same, while the long-lived component (τ_2) decreased from 4.75 ns to 2.50 ns (Table S2). The decrease of the long-lived lifetime may be ascribed to dynamic quenching by free $(TBA)_3PO_4$. Fluorescence decay for cage 1^{Me} was also measured in acetonitrile for the comparison with host-guest complexes. The lifetimes of cage 1^{Me} are lengthened in acetonitrile (from 0.41 ns to 0.63 ns for τ_1 , and 2.50 ns to 6.30 ns for τ_2) duo to the influence of solvent polarity.

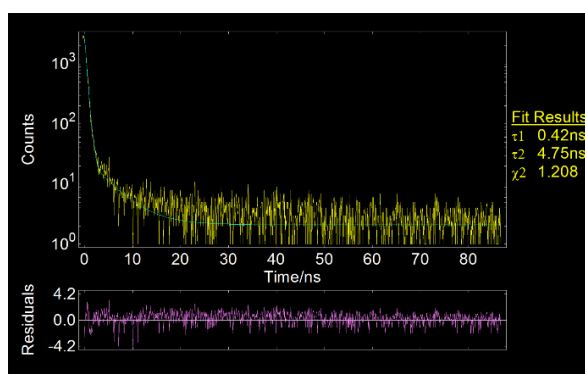


Figure S32. Fluorescence emission decays of L^{Me} ($\lambda_{em} = 380$ nm, 40 μ M in DMSO).

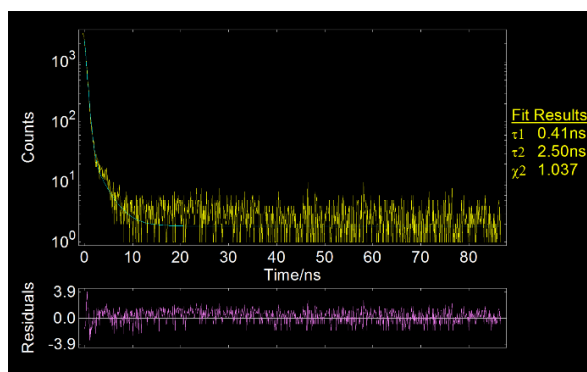


Figure S33. Fluorescence emission decays of (TBA)₁₂[(PO₄)₄(L^{Me})₄] (cage **1**^{Me}, $\lambda_{\text{em}} = 381\text{ nm}$, 10 μM in DMSO).

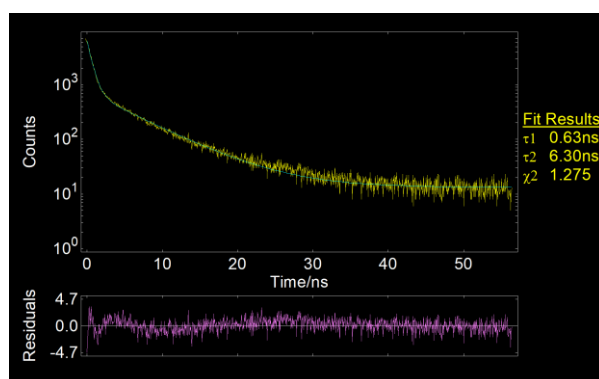


Figure S34. Fluorescence emission decays of (TBA)₁₂[(PO₄)₄(L^{Me})₄] (cage **1**^{Me}, $\lambda_{\text{em}} = 381\text{ nm}$, 10 μM in acetonitrile).

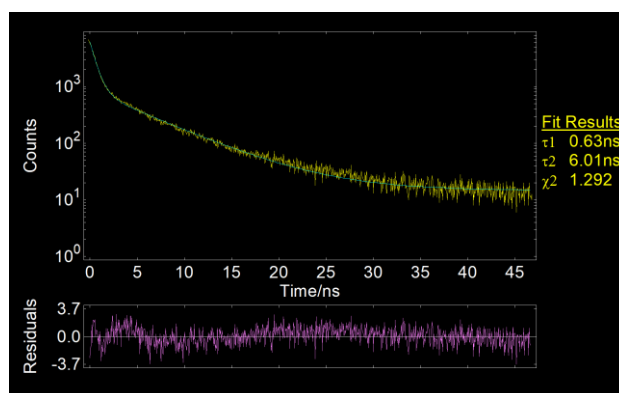


Figure S35. Fluorescence emission decays of Cage **1**^{Me}-C(CH₃)₃Cl ($\lambda_{\text{em}} = 381\text{ nm}$, 10 μM in acetonitrile).

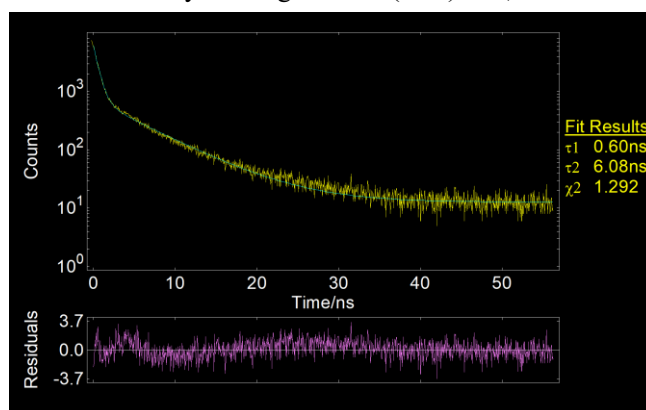


Figure S36. Fluorescence emission decays of Cage **1**^{Me}-TMA⁺ ($\lambda_{\text{em}} = 381\text{ nm}$, 10 μM in acetonitrile).

Table S2. Lifetimes (τ_i) of L^{Me} and Cage 1^{Me} ((TBA)₁₂[(PO₄)₄(L^{Me})₄]), Cage $1^{Me}\rightarrow C(CH_3)_3Cl$ and Cage $1^{Me}\rightarrow TMA^+$.

Complex	Component (τ_i)	τ_i (ns)
L^{Me} [a]	(τ_1)	0.42(91.85)
	(τ_2)	4.75(8.15)
Cage 1^{Me} [a]	(τ_1)	0.41(91.61)
	(τ_2)	2.50(8.39)
Cage 1^{Me} [b]	(τ_1)	0.63(45.17)
	(τ_2)	6.30(54.83)
Cage $1^{Me}\rightarrow C(CH_3)_3Cl$ [b]	(τ_1)	0.63(41.16)
	(τ_2)	6.01(58.84)
Cage $1^{Me}\rightarrow TMA^+$ [b]	(τ_1)	0.60(44.39)
	(τ_2)	6.08(55.61)

[a] Measured in DMSO, [b] measured in acetonitrile.

Table S3. Fluorescence quantum yield of L^{Me} , Cage 1^{Me} ((TBA)₁₂[(PO₄)₄(L^{Me})₄]), Cage $1^{Me}\rightarrow C(CH_3)_3Cl$ and Cage $1^{Me}\rightarrow TMA^+$ and L^{NO_2} .

Complex	Quantum yield (Φ , %)
L^{Me} [a]	42.5
Cage 1^{Me} [a]	3.3
Cage 1^{Me} [b]	3.6
Cage $1^{Me}\rightarrow C(CH_3)_3Cl$ [b]	13.7
Cage $1^{Me}\rightarrow TMA^+$ [b]	0.8
L^{NO_2} [a]	< 0.1

[a] Measured in DMSO, [b] measured in acetonitrile.

S5. UV-vis property

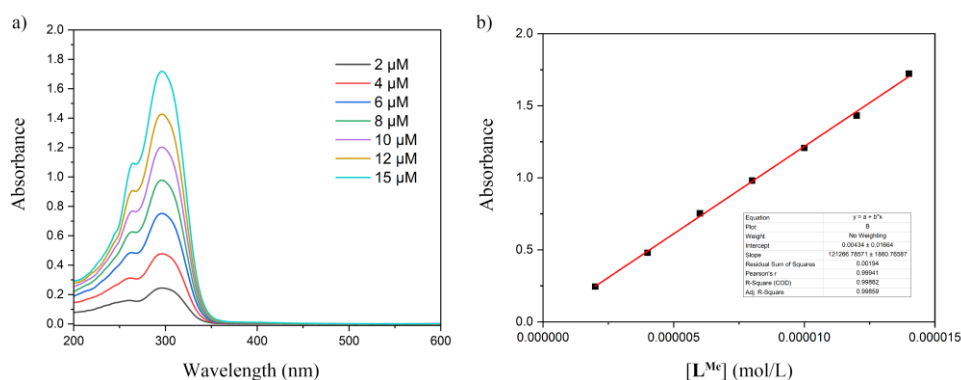


Figure S37. a) UV-vis absorption spectra of L^{Me} with different concentrations in DMSO, b) plots of UV-vis intensity (295 nm) vs $[L^{Me}]$, the extinction coefficient of L^{Me} was determined as $(1.21 \pm 0.02) \times 10^6 \text{ M}^{-1} \text{ cm}^{-1}$.

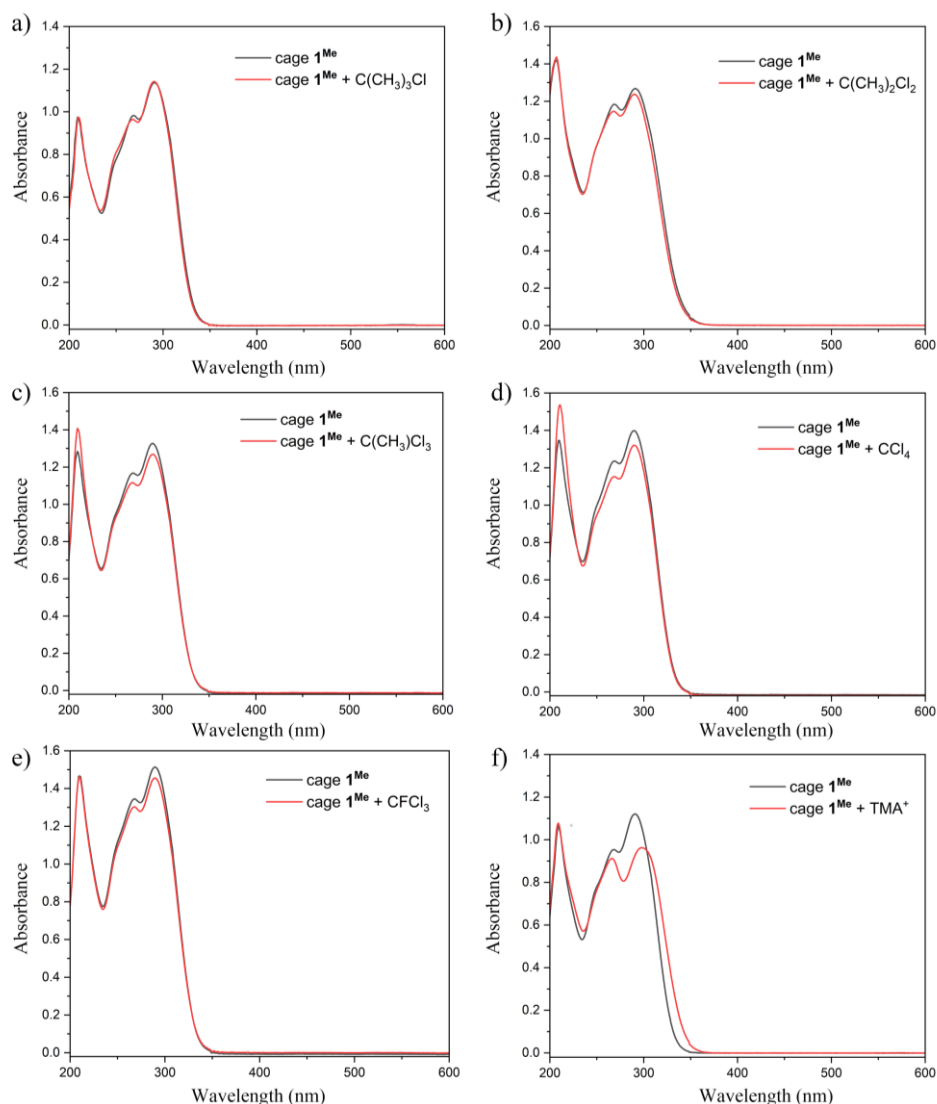


Figure S38. UV-vis spectra (2.5 μM in CH_3CN) of a) cage $\mathbf{1}^{\text{Me}}$ and cage $\mathbf{1}^{\text{Me}}$ with $\text{C}(\text{CH}_3)_3\text{Cl}$, b) cage $\mathbf{1}^{\text{Me}}$ and cage $\mathbf{1}^{\text{Me}}$ with $\text{C}(\text{CH}_3)_2\text{Cl}_2$, c) cage $\mathbf{1}^{\text{Me}}$ and cage $\mathbf{1}^{\text{Me}}$ with $\text{C}(\text{CH}_3)\text{Cl}_3$, d) cage $\mathbf{1}^{\text{Me}}$ and cage $\mathbf{1}^{\text{Me}}$ with CCl_4 , e) cage $\mathbf{1}^{\text{Me}}$ and cage $\mathbf{1}^{\text{Me}}$ with CFCl_3 , f) cage $\mathbf{1}^{\text{Me}}$ and cage $\mathbf{1}^{\text{Me}}$ with TMA^+ . All the guest molecules were in a saturated state.

S6. X-ray crystallography

Diffraction data were collected on Rigaku XtaLAB Pro diffractometer with Cu-K α radiation ($\lambda = 1.54178 \text{ \AA}$) at 100 K. An empirical absorption correction using SADABS was applied for all data. The structures of cage $\mathbf{1}^{\text{Me}}$ were solved by dual space using the SHELXT program. All non-hydrogen atoms were refined anisotropically by full-matrix least-squares on F^2 by the use of the SHELXL program. Hydrogen atoms bonded to carbon and nitrogen were included in idealized geometric positions with thermal parameters equivalent to 1.2 times those of the atom to which they were attached. The site occupancy factors of $\text{C}_3\text{H}_6\text{O}$ inside the cage were refined. The final site occupancy factors for $\text{C}_3\text{H}_6\text{O}$ in $\mathbf{1}^{\text{Me}} \supset \text{C}_3\text{H}_6\text{O}$ is 0.68.

One aryl rings for $\mathbf{1}^{\text{Me}}\supset\text{C}_3\text{H}_6\text{O}$ were refined with restraints. Two TBA⁺ counter cation in $\mathbf{1}^{\text{Me}}\supset\text{C}_3\text{H}_6\text{O}$ were refined with restraints.

The remaining solvents could not be successfully resolved despite numerous attempts at modeling, and consequently the SQUEEZE function of PLATON was required to account for these highly disordered solvents. The removed void electron density corresponds to about 26 water molecules for $\mathbf{1}^{\text{Me}}\supset\text{C}_3\text{H}_6\text{O}$ per cage.

Due to the moderate quality of the diffraction data, amount of the TBA⁺ molecules could not be completely located. In addition, some twisty aryl rings and the highly disordered TBA⁺ molecules of $\mathbf{1}^{\text{Me}}\supset\text{C}_3\text{H}_6\text{O}$ caused the alerts level B in the checkCIF report. The difference between the given and expected formula weight caused the alerts level c in the checkCIF report.

CCDC 2218391 contain the supplementary crystallographic data for this paper. These data can be obtained free of charge from The Cambridge Crystallographic Data Centre via www.ccdc.cam.ac.uk/data_request/cif.

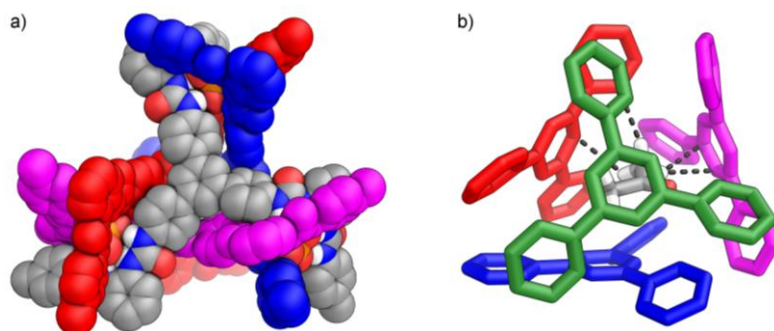


Figure S39. Crystal structure of the tetrahedral cage $[(\text{PO}_4)_4 \text{L}^{\text{Me}}_4]^{12-}$ with an encapsulated acetone.

Table S4. Crystal data of $\mathbf{1}^{\text{Me}}\supset\text{C}_3\text{H}_6\text{O}$.

	$\mathbf{1}^{\text{Me}}\supset\text{C}_3\text{H}_6\text{O}$
Empirical formula	$\text{C}_{470.03}\text{H}_{676.06}\text{N}_{60}\text{O}_{40.68}\text{P}_4$
Formula weight	7941.81
Crystal System	Orthorhombic
Space group	$P2_12_12_1$
a (Å)	31.4137(3)
b (Å)	32.1377(2)
c (Å)	50.4723(4)
α (deg)	90
β (deg)	90
γ (deg)	90
V (Å ³)	50955.0(7)
Z	4
D_{calc} , g/cm ³	1.035

Flack parameter	0.383(14)
No. of unique data	97172
T (K)	100(2)
Total no. of data	241157
Crystal size (mm)	0.10 x 0.10 x 0.10
θ range	2.153 to 73.126
Completeness to θ	99.8 %
Goodness-of-fit on F^2	1.058
$R1$	0.0909
$wR2$	0.2505

Table S5. Hydrogen bonds around the PO_4^{3-} ions in $\mathbf{1}^{\text{Me}}\text{C}_3\text{H}_6\text{O}$.

PO_4	D–H \cdots A	$d(\text{D–H})$	$d(\text{H}\cdots\text{A})$	$d(\text{D}\cdots\text{A})$	$\angle(\text{DHA})$
P1	N21–H21 \cdots O27	0.88	2.07	2.917(3)	161
	N22–H22A \cdots O25	0.88	1.95	2.761(3)	152
	N23–H23A \cdots O25	0.88	1.90	2.777(3)	175
	N24–H24 \cdots O28	0.88	1.99	2.796(3)	152
	N33–H33A \cdots O27	0.88	2.22	2.814(3)	124
	N24–H34 \cdots O26	0.88	1.92	2.771(3)	163
	N35–H35 \cdots O26	0.88	1.91	2.786(3)	173
	N36–H36A \cdots O25	0.88	1.95	2.792(3)	161
	N45–H45 \cdots O27	0.88	1.98	2.823(3)	161
	N46–H46A \cdots O28	0.88	1.98	2.810(3)	156
	N48–H48 \cdots O26	0.88	1.98	2.813(4)	158
	N47–H47A \cdots O28	0.88	1.88	2.752(4)	169
P2	N9–H9A \cdots O31	0.88	2.09	2.793(3)	136
	N10–H10 \cdots O30	0.88	1.96	2.793(3)	157
	N11–H11A \cdots O30	0.88	1.93	2.798(3)	168
	N12–H12A \cdots O29	0.88	1.94	2.803(3)	165
	N13–H13 \cdots O31	0.88	2.03	2.825(2)	149
	N14–H14 \cdots O29	0.88	1.96	2.777(3)	154
	N15–H15A \cdots O29	0.88	1.89	2.759(3)	169
	N16–H16A \cdots O32	0.88	1.95	2.793(3)	160
	N29–H29A \cdots O31	0.88	2.07	2.892(3)	155
	N30–H30A \cdots O32	0.88	1.96	2.802(3)	160
	N31–H31 \cdots O32	0.88	1.91	2.767(3)	163
N32–H32A \cdots O30	0.88	1.96	2.824(3)	165	
P3	N1–H1A \cdots O34	0.88	2.02	2.822(3)	151
	N2–H2 \cdots O33	0.88	2.02	2.849(3)	156
	N3–H3A \cdots O33	0.88	1.89	2.762(3)	173

	N4–H4...O35	0.88	2.00	2.832(3)	157
	N25–H25A...O34	0.88	2.09	2.938(3)	162
	N26–H26A...O35	0.88	1.92	2.744(3)	155
	N27–H27...O35	0.88	1.93	2.793(3)	167
	N28–H28...O36	0.88	1.97	2.840(3)	168
	N41–H41...O34	0.88	2.17	2.945(3)	146
	N44–H44A...O33	0.88	1.96	2.819(3)	165
	N42–H42...O36	0.88	2.01	2.752(3)	141
	N43–H43A...O36	0.88	1.89	2.761(3)	171
P4	N5–H5A...O38	0.88	2.07	2.895(3)	155
	N6–H6...O40	0.88	2.00	2.791(3)	148
	N7–H7...O40	0.88	1.88	2.750(3)	169
	N8–H8A...O39	0.88	1.94	2.766(3)	156
	N17–H17A...O38	0.88	2.04	2.867(3)	155
	N18–H18A...O37	0.88	1.96	2.765(3)	152
	N19–H19...O37	0.88	1.94	2.798(3)	167
	N20–H20...O40	0.88	2.04	2.866(3)	156
	N37–H37A...O38	0.88	2.04	2.812(3)	146
	N38–H38A...O39	0.88	1.90	2.762(3)	165
	N39–H39A...O39	0.88	1.93	2.795(3)	166
	N40–H40...O37	0.88	1.97	2.809(3)	160

S7. High-Resolution MS Study

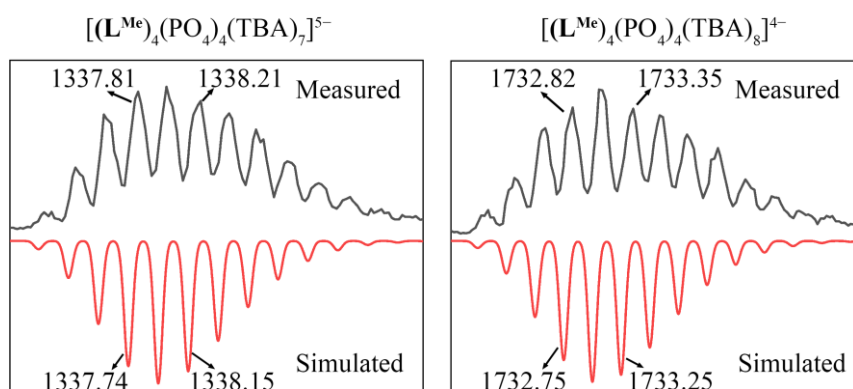


Figure S40. The high-resolution ESI-spectra of $(L^{Me})_4(PO_4)_4(TBA)_{12}$ in different valences.

S8. Reference

1. D. Yang, J. Zhao, Y. Zhao, Y. Lei, L. Cao, X.-J. Yang, M. Davi, N. d. S. Amadeu, C. Janiak, Z. Zhang, Y.-Y. Wang and B. Wu, *Angew. Chem. Int. Ed.*, 2015, **54**, 8658-8661.
2. H. Takezawa, T. Murase, G. Resnati, P. Metrangolo and M. Fujita, *J. Am. Chem. Soc.*, 2014, **136**, 1786-1788.